Mechanics and Mechanical Engineering
Vol. 20, No. 4 (2016) 377–392

Comparision of Experimental and Simulated Weld Bead Geometry by Varying the Weld Speed in TIG Welded AA7075 Aluminium Alloy

S. Amal Bosco Jude
Department of Mechanical Engineering
University VOC College of Engineering
Thoothukudi, Tamilnadu 628 008, India
sabjude81@rediffmail.com

G. R. Jinu
P. Arul Franco
Department of Mechanical Engineering
University College of Engineering
Nagercoil, Tamilnadu 629 004, India

Received (22 May 2016)
Revised (16 July 2016)
Accepted (24 September 2016)

In this present study, Aluminium Alloy material (AA7075) is selected as the investigation material in which TIG welding process was utilized for welding and the temperature analysis was carried out. The same was simulated using ANSYS software by finite element technique considering the characteristics and advantage of TIG welding process than other sources for welding of aluminium alloys. A travel heat source combined with body loads was designed by analyzing thermal physical parameters, latent heat of fusion of material. The weld model was created by using Solid modeling and direct generation technique. Residual control method was taken for precise node selection. The simulation was carried out by varying the welding speed process parameter of TIG welding and keeping current & voltage as constant. The quasisteady state temperature field of TIG welding was simulated with the FEA software (ANSYS) as well as experimental tests. The main objective of this work is to compare the experimentally obtained weld bead geometry parameters such as bead width and depth of penetration of AA7075 welded joint with simulated results from ANSYS software for various weld speeds. From the results it is indentified that for the sample welded at 120 mm/min is having higher weld bead geometry when compared to the samples welded at 130 mm/min and 140 mm/min. The lower bead geometry is obtained for the sample welded at 140 mm/min is due to the application of less heat energy as input. Similarly for 130 mm/min lower bead geometry is obtained because less heat energy is spent on joining. Joining of two metals or alloys is important in every aspect of engineering which leads to welding in an effective manner and carrying out the analysis. The experimental analysis shows that the model is showing good agreement with the experimental results. Comparison of the

experimental and simulated results shows the maximum deviation of 6.24 % and 6.28 % is obtained for calculating the bead width and depth of penetration, respectively.

Keywords: TIG welding, AA7075, Simulation, Weld Bead Geometry, ANSYS.

1. Introduction

In Fusion welding heating was applied by the an intense heat source by which melting and solidification of parent metals was happened and filler material was also added if required in the localized fusion zone. These heat sources causes non uniform temperature distributions across the joint and the parent metals. In order to analyze the effect of heat source on the weld pool dimension, The computational weld pool models were developed [1–4]. Some of the researchers concentrated in predicting the weld thermal cycles and fluid flow pattern of welding process was developed using finite element method. [5–7]. Therefore finite element was used to analyze the compleity of welding process itself and the complex geometry of real engineering components to predict the weld thermal cycle and corresponding flow field which are very difficult task in experimental analysis. In related to this, the accuracy of these quantitative calculations was mainly depend on the accuracy of various input parameters. Since few of the input process parameters are uncertain in nature. Hence various optimization algorithms are linked with numerical process models to overcome these uncertainities [8].

As stated in literatures [9&10], it is very difficult to measure the temperature at the weld pool using thermocouple, because of small of the weld pool and high temperature developed during welding process. Therefore it is difficult to place the thermocouple in the weld pool. These problems can be overcome using indirect techniques such as infrared cameras etc. which also includes high degree of uncertainity due to many assumptios such as associated angle and wavelength etc, therefore it is very difficult to identify a reliable technique available for measuring the temperature within the molten weld pool [11].

Lot of analytical solutions was developed for fusion welding using governing partial differentiation of conservation of energy. In this various non linearity problems was arising due to the temperature dependent material properties, radiant heat transfer at the boundary and complex geometry which further creates problems in solving these problems by analytical methods. But the analytical models are still used in predicting the weld pool dimensions and cooling rates which can be computed faster. In analytical solutions the temperature distributions was depend on the following considerations such as weld arc as a point heat source, assumption of constant material properties and the neglect of latent heat [12–14]. The accuracy of the analytical solutions in predicting the transient temperature fields mainly depends on the assumptions made in the analytical models. To overcome these difficulties, numerical models were developed in which the distributed heat source is considered as the Gaussian distribution in contrast to the point heat source in which difficulties are faced in assuming the heat transfer mode. Therefore a volumetric heat source of ellipsoidal or double ellipsoidal shape was developed by taking consideration of the heat transport inside the weld pool [15–17].

DebRoy et al. modelled a convective heat transport in weld pool through the solution of continuity, momentum and energy equations. They also used three–

dimensional heat transfer and fluid flow analysis based on finite volume method to model heat transfer and fluid flow in weld pool [18 &19].

Durgutlu [20] has investigated the effect of hydrogen in argon as shielding gas for TIG welding of 316L austenitic stainless steel. The microstructure, penetration and mechanical properties were examined. The conclusion given in the investigation was that the mean grain size in the weld metal along with its penetration depth and width is increased with increasing hydrogen content.

Jun Yan et al. [21] studied the microstructure and mechanical properties of 304 stainless steel joints by TIG welding, laser welding and laser–TIG hybrid welding process. Then, the tensile tests were performed and the fracture surfaces were analysed. From the various test results, it is observed that the laser welding and hybrid welding are suitable to weld 304 stainless steel due to their high welding speed and excellent mechanical properties.

Sathiya et al [22] conducted an experiment on TIG welded duplex stainless steel to investigate the role of shielding gas on metallurgical and mechanical properties. Here, the helium and argon shielding gas were used. After performing the mechanical and metallurgical testing it is observed that the He–shielded weld bead aspect ratio is higher than Ar–shielded weld and the hardness of the weld metal is much higher than that of the BM and HAZ for both shielding gases.

Therefore from the literatures it is identified that lot of work has been already developed in predicting the temperature distribution of the fusion welding using various mathematical models and analytical solutions by considering various assumptions. The accuracy of these models is questionable due to the various assumptions. Similarly from the literatures it is also noted that, measuring the temperature in the weld pool using thermocouple is very difficult. The main objective of this work is to compare the experimentally obtained weld bead geometry parameters such as bead width and depth of penetration of AA7075 welded joint with simulated results from ANSYS software for various weld speeds such as 120 mm/min, 130 mm/min, 140 mm/min).

2. Mathematical model

The TIG welding process simulation starts by estimating the temperature profiles using a moving heat source because the thermal strains developed loads the welded structure due to uncontrolled expansion and contraction which is associated with the non-uniform temperature distribution. In this work transient thermal analysis is considered for determining the temperatures and other thermal quantities for time varying thermal loads. The welding process is taken as non-linear by considering the temperature dependent material properties [1].

The mathematical formulation for three-dimensional heat conduction in a domain $D$is given as follows (1):

$$\frac{\partial}{\partial x}\left(K_x \frac{\partial T}{\partial x}\right) + \frac{\partial}{\partial y}\left(K_y \frac{\partial T}{\partial y}\right) + \frac{\partial}{\partial z}\left(K_z \frac{\partial T}{\partial z}\right) + q_v\,(x, y, z) = \rho c_p \left(\frac{\partial T}{\partial t} + (-v_w)\frac{\partial T}{\partial x}\right) \tag{1}$$

where: Q is the power generation per unit volume in the domain D, Wm^{-3}; K_x, K_y, K_z is the thermal conductivity in x, y, and z directions, $\mathrm{Wm}^{-1}\mathrm{K}^{-1}$; c is the specific heat capacity, $\mathrm{Jkg}^{-1}\mathrm{K}^{-1}$; ρ is the density of the material, kgm^{-3}; t is the time, s; and V is the velocity of moving source, m/s.

The initial condition is:

$$T\,(x, y, z, o) = T_0 \quad \text{for} \quad (x, y, z) \in D \tag{2}$$

The essential boundary condition is:

$$T\,(o, y, z, t) = T_0 \tag{3}$$

On the boundary S_1 for $(y, z) \in S_1$ and $t > 0$.
This condition prescribes nodal temperatures at the flow inlet. The natural boundary condition can be defined by

$$K_n \frac{\partial T}{\partial n} q + h(T - T_0) + \sigma\varepsilon(T^4 - T_0^4) = 0 \tag{4}$$

On the boundary S_2 for $(x,\ y,\ z)$ S_2 and $t > 0$, where S_1 represents the inlet surface; S_2 represents those surfaces that are subjected to convection and imposed heat fluxes; K_n is the thermal conductivity normal to the surface, $\mathrm{Wm}^{-1}\mathrm{K}^{-1}$; q is the prescribed heat flux, Wm^{-2}; h is the convection heat transfer coefficient, $\mathrm{Wm}^{-2}\mathrm{K}^{-1}$; T_o is the ambient temperature, K; σ is the Stephan–Boltzman constant for radiation 5.67×10^{-8} Wm^{-2} k^{-4} and ε is the emissivity.

3. Material properties

Aluminium Alloy AA7075 contains 5.62 % zinc, 2.32 % magnesium and 1.28 % copper. The addition of zinc controls the grain structure which inturn results in stronger alloy. Aluminium alloy 7075 is a high strength alloy with excellent corrosion resistance. It has the highest strength of the 7000 series alloys. Alloy 7075 is known as a structural alloy. In plate form, Aluminium alloy 7075 is the alloy most commonly used for machining. As a relatively new alloy, the higher strength of Aluminium alloy 7075 is used to replace 6000 series in many applications. The maximum melting point of AA7075 is 635 $^\circ$C. The chemical composition of AA7075 is given in Tab. 1. The temperature dependent material property(thermal conductivity, specific heat and density) used in this work are given in Tab. 2 and shown in Fig. 1 (a, b and c) respectively.

4. Experimental work

In this study, the size of the AA 7075 aluminium alloy base material chosen for this investigation was $150{\times}75{\times}3$ mm^3 sheets are welded to each other by automatic TIG welding process as shown in Fig. 2 and 3.

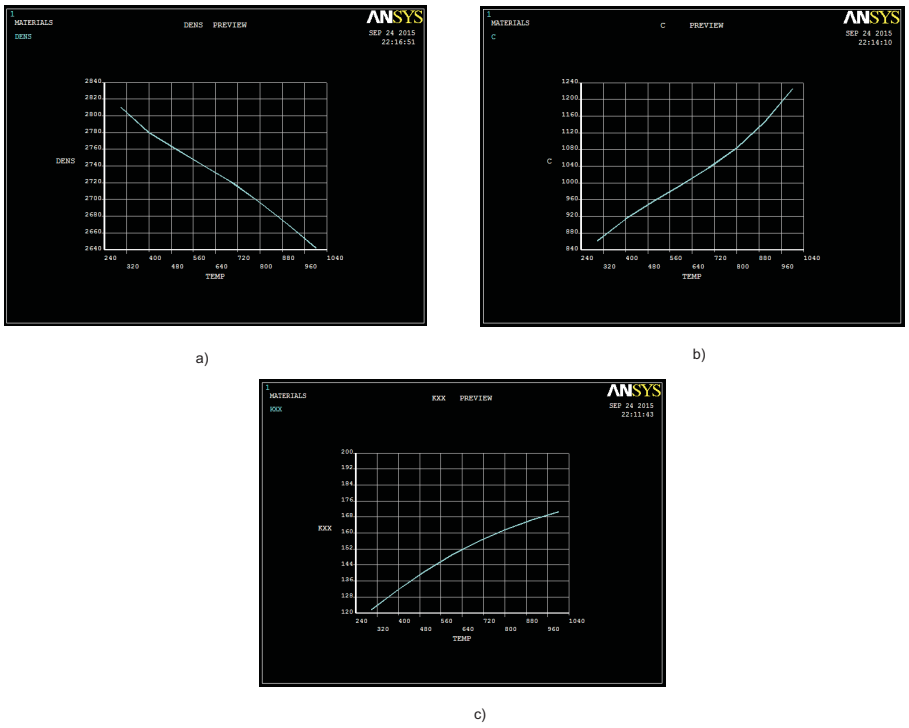

Figure 1 a)Temperature versus Density for AA7075, b)Temperature versus Specific Heat, c)Temperature versus Thermal Conductivity (Kxx) for AA7075

Table 1 Chemical composition of AA7075 aluminium alloy (wt%)

Alloy	Mg	Si	Fe	Cr	Cu	Mn	Ti	Zn	Al
AA7075	2.32	0.10	0.30	0.21	1.28	0.12	0.02	5.62	Balance

Table 2 Temperature dependent material property data for a Aluminium Alloy 7075

Sl.No.	Temperature K	Thermal conductivity W/m-K	Specific Heat J/Kg-K	Density (g/cm^3)
1	300	121.62	862	2.810
2	400	131.69	913	2.780
3	500	140.74	955	2.760
4	600	148.75	994	2.740
5	700	155.74	1036	2.720
6	800	161.70	1084	2.696
7	900	166.63	1146	2.670
8	1000	170.53	1225	2.642

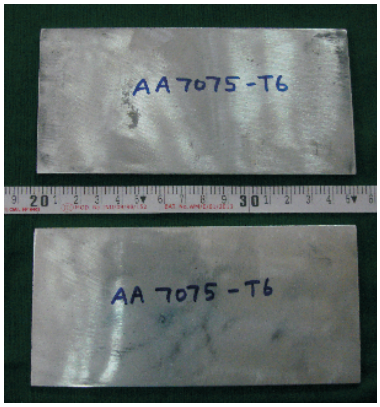

Figure 2 Macro image of base material

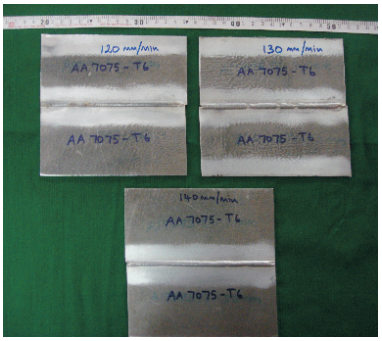

Figure 3 Macro image of the welded samples before welding at various speeds

Table 3 Welding process parameters

Specimen No.	Current (Amps)	Voltage (V)	Weld speed mm/min	Heat input (kJ/mm)	Feed rate of filler metal (mm/min)	Gas flow rate (l/min)
Sample 1	170	16	120	1.360	350	12
Sample 2	170	16	130	1.255	350	12
Sample 3	170	16	140	1.165	350	12

The butt welding process was performed with 5356 filler metal at different weld speeds. The welding process parameters are given in Tab. 3.

After welding, the samples were cooled in the air and subjected to radiography testing. The radiography test result reveals that the welded samples are free from defects. Three specimens were prepared from each welded samples for the welding speeds of 120, 130 and 140 mm/min. The weld samples were cut in to pieces for macrostructural examination to study the bead geometry as shown in Fig. 4.

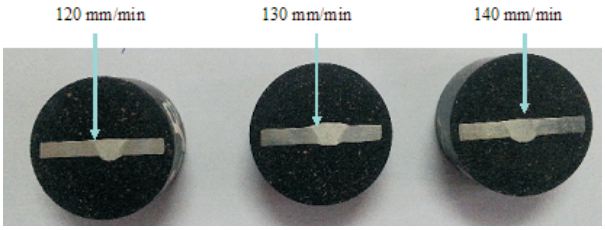

Figure 4 Samples for macrostructural examination

5. Finite element model

In TIG welding process, the heat input applied for joining the materials sometimes may result in serious metallurgical changes in the welded structure, which may lead to the early failure of the component. This thermal cycle creates way for various analyses like prediction of distortion and residual stresses, metallurgical analyses etc. Therefore, it is necessary to study the heat flow temperature distribution in the welded joints. The development in the computing and numerical techniques like Finite Element Analysis (FEM) has made it possible to model complicated configurations and loading conditions which are difficult in earlier stages. Therefore, Computer–based simulations offer the possibility to examine the different aspects of the process without having a physical prototype of the product [19].

In this work, the main parameters of TIG welding process are considered, and the finite element simulation is performed using ANSYS version R.15.0. The material used for the study is Aluminium Alloy 7075.

The material properties of Aluminium Alloy 7075 like thermal conductivity, density and specific heat used in this work are given in Table 2 and Figures 1(a-c) [23]. These temperature dependent material properties are taken as an input value for this simulation work. This work was carried out by using ANSYS version R.15.0 software to simulate the temperature distribution of the weldments.

The convection film coefficient that covers the effect of convection and radiation is obtained from the equation $h = 2.41 \times 10^{-3} T_{1.61}$ (W/m^2 ^{o}C) [19]. All the properties are considered to be temperature dependent and listed in literature

From the specific heat listed in the table, enthalpy values are calculated, taking into account the latent heat of fusion in the melting temperature range.

5.1. *Definition of boundary and initial condition*

Natural convection occurs on all the surfaces of the sheet other than the bottom surface. The region below the arc experiences forced convection due to the flow of the shielding gas (Argon) which is supplied at 15 l/min in the experimental investigation. The effect of forced convection is not taken into account in the finite element simulation. Combined convection and radiation are considered by Vinokurov's empirical relationship:

$$h = 2.41 \times 10^{-3} \varepsilon T_{1.61} \text{ (W/m}^2\,^o\text{C)} \tag{5}$$

where ε is the surface emissivity $\varepsilon = 0.285$ for AA7075 Aluminium Alloy. Temperature dependent values of thermal conductivity are being considered. The ambient temperature is applied as initial temperature for the weld sheet in the transient thermal analysis [19].

5.2. *Creation of FEM Model*

In this work, the model is generated using direct generation techniques in solid modelling with the help of geometric primitives, which are fully developed lines, areas and volume as shown in Figs. 5 and 6. The solid model is meshed using solid70 directly. Along the depth direction one element is used. Along the welding direction 150 divisions are made and in transverse directions 71 divisions are made as shown in Fig. 7.

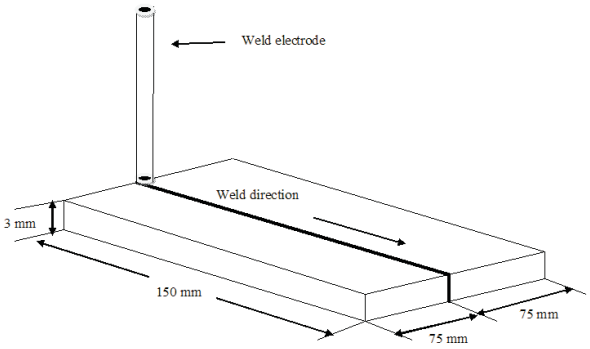

Figure 5 Geometric representation of the Weld Plate model

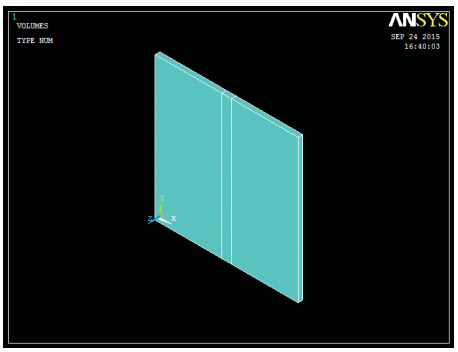

Figure 6 Weld plate model using ANSYS for AA7075 weldments

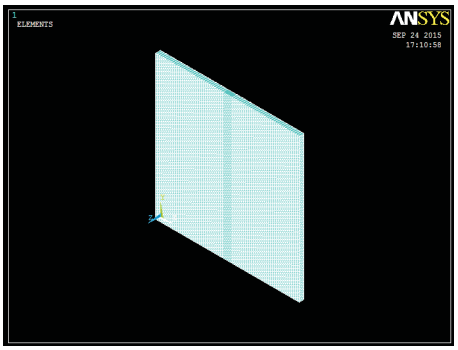

Figure 7 Meshed model using ANSYS for AA7075 weldments

6. Results and discussions

The experimental work is conducted based on the chosen parameter as shown in Tab. 3. After welding, the weld bead geometry (weld bead width and depth of penetration) is measured and the values presented in Tab. 4, the corresponding figures are shown in Fig. 8.

Table 4 Experimental results of weld bead geometry for AA7075 welded joints on various TIG welding process parameter

Specimen No.	Current Amps	Voltage V	Weld speed mm/min	Heat input (kJ/mm)	Bead width (mm)	Bead depth (mm)
Sample 1	170	16	120	1.360	7.85	4.46
Sample 2	170	16	130	1.255	7.31	4.21
Sample 3	170	16	140	1.165	7.02	4.10

From Tab. 4, it is identified that maximum bead width and bead depth are obtained for the samples welded at 120 mm/min. The samples welded at 130 mm/min and 140 mm/min have lower bead geometry than at 120 mm/min because in the sample welded at 140 mm/min lower heat input is applied which is insufficient and only surface melting takes place which results in distortion in the weld plate. Similarly, the sample welded at 130 mm/min experiences low heat input in which less heat is spent in welding. Therefore, from the experimental result it is clearly understood that heat input plays a major role in welding in which lower heat input affects the quality of the welded joints. Therefore, optimum heat input is preferred in joining of metals.

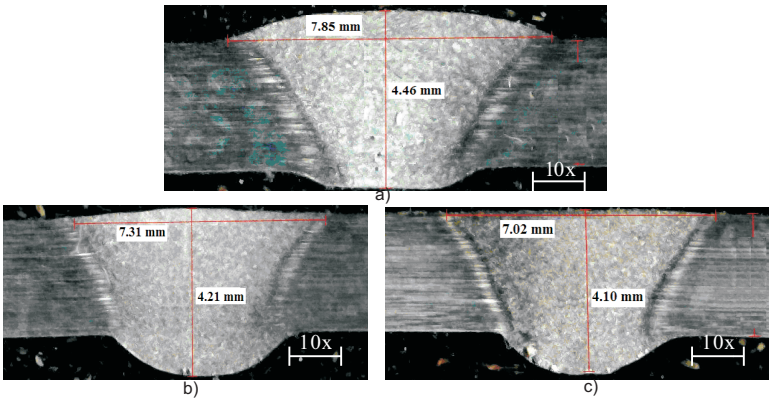

Figure 8 a) Weld bead profile for AA7075 weldments at the speed of 120 mm/min, b) Weld bead profile for AA7075 weldments at the speed of 130 mm/min, c) Weld bead profile for AA7075 weldments at the speed of 140 mm/min

In the present work, it is very important to find the temperature distribution during TIG welding process in AA7075 sheet in order to find the bead width and bead depth of the welded joints. To attain the objective of this work, the welding speed was varied from 120–140 mm/min with an interval of 10 mm/min and the corresponding thermal cycles experienced on the input process varying from 1.165–1.360 kJ/mm. The transient thermal analysis was performed using Finite Element Method. The thermal cycles at various places from the weld and the temperature distributions for various time intervals were analysed. From the simulated results the corresponding weld bead geometry was also measured. The simulation work was carried out using ANSYS R.15.0 and the results are compared with the experimental results.

The simulation of the TIG welding process in AA7075 sheet was carried out using ANSYS R.15.0 with the following various input parameters as given in Table 3 and the results are given in Tab. 5. The simulated images for 120 mm/min are shown in Fig. 9a, b and Fig. 10. Similarly, the simulated image of 130 mm/min is shown in Fig. 11 and Fig. 12. The simulated image of 140 mm/min is shown in Fig. 13 and Fig. 14.

Table 5 Simulated results of weld bead geometry for AA7075 welded joint on various TIG welding process parameters

Specimen No.	Current (Amps)	Voltage (V)	Weld speed mm/min	Heat input (kJ/mm)	Bead width (mm)	Bead depth (mm)
Sample 1	170	16	120	1.360	7.36	4.18
Sample 2	170	16	130	1.255	7.02	4.03
Sample 3	170	16	140	1.165	6.83	3.94

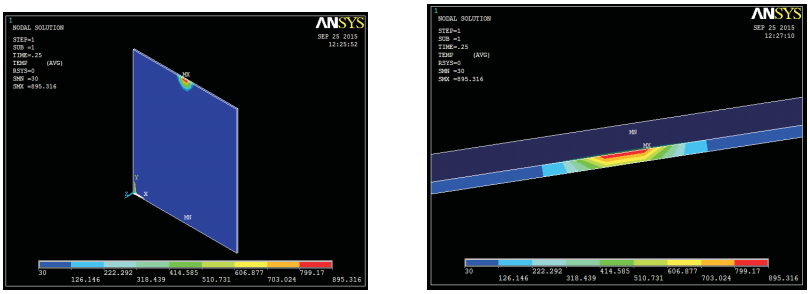

Figure 9 a)Temperature contour plot of AA7075 for bead on plate weld at 120 mm/min for 0.25 sec, b)Temperature contour plot of AA7075 for weld bead geometry along thickness at 120 mm/min for 0.25 sec

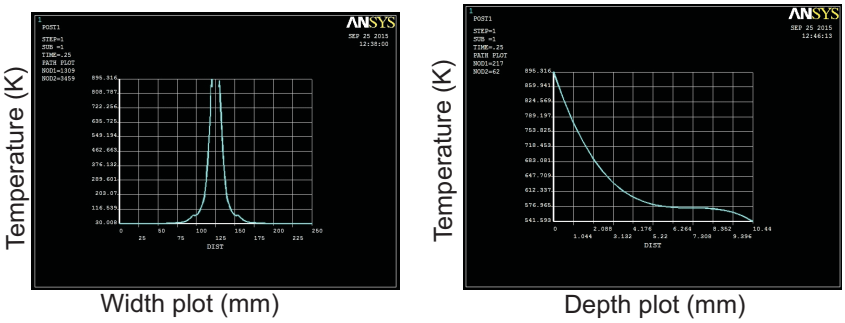

Figure 10 a) Temperature Vs Width plot of AA7075 for bead on plate weld at 120 mm/min for 0.25 sec, b)Temperature Vs Depth plot of AA7075 for weld bead geometry thickness at 120 mm/min for 0.25 sec

The Fig. 9 shows the temperature distribution of bead on plate weld along with the width and depth of the plate welded at 120 mm/min. and heat input of 1.360 kJ/mm applied for 0.25 sec time step at single node and the results are captured.

Fig. 10 shows the temperature versus width and depth of the welded plate graph. In this 908 k is the melting temperature of AA7075 Aluminium alloy. From Figure 10 (a) the bead width of 7.36 mm and Figure 10 (b) bead depth of 4.18 mm are identified.

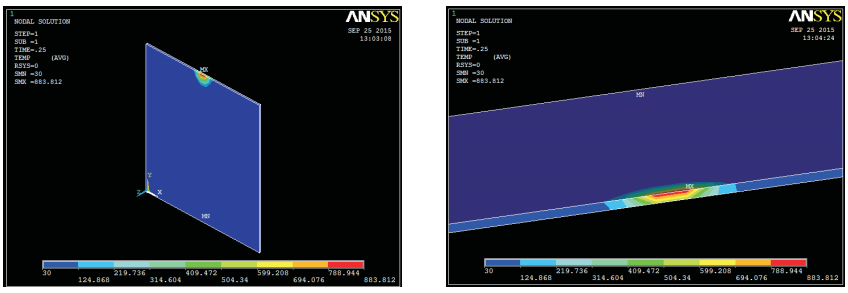

Figure 11 a)Temperature contour plot of AA7075 for bead on plate weld at 130 mm/min for 0.25 sec, b)Temperature contour plot of AA7075 for weld bead geometry along thickness at 130 mm/min for 0.25 sec

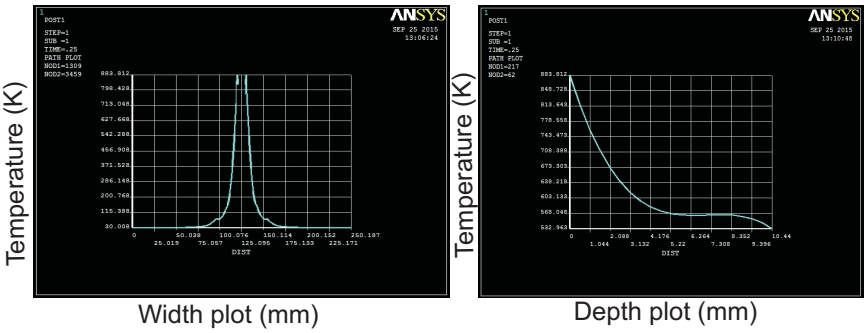

Figure 12 a)Temperature Vs Width plot of AA7075 for bead on plate weld at 130 mm/min for 0.25 sec,a)Temperature Vs Width plot of AA7075 for bead on plate weld at 130 mm/min for 0.25 sec, b) Temperature Vs depth plot of AA7075 for weld bead geometry thickness at 130 mm/min for 0.25 sec

Fig. 11 shows the temperature distribution of bead on plate weld along with the width and depth of the plate welded at 130 mm/min. and heat input of 1.255 kJ/mm applied for 0.25 sec time step at single node and the results are captured. Fig. 12 shows the temperature versus width and depth of the welded plate graph. In this 908 k is the melting temperature of AA7075 Aluminium alloy. From Fig. 12a the bead width of 7.02 mm and Fig. 12b bead depth of 4.03 mm are identified.

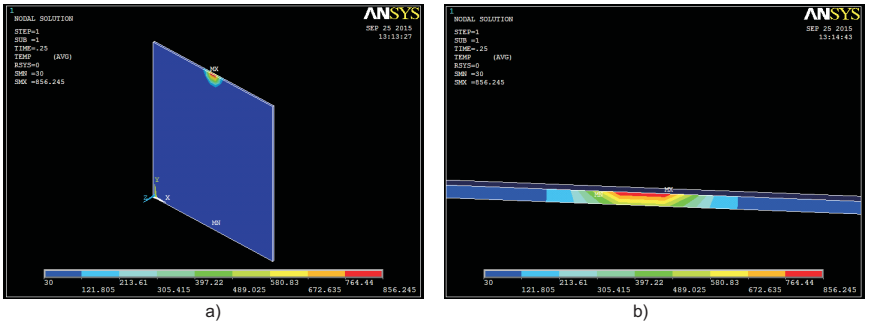

Figure 13 a)Temperature contour plot of AA7075 for bead on plate weld at 140 mm/min for 0.25 sec, b)Temperature contour plot of AA7075 for weld bead geometry along thickness at 140 mm/min for 0.25 sec

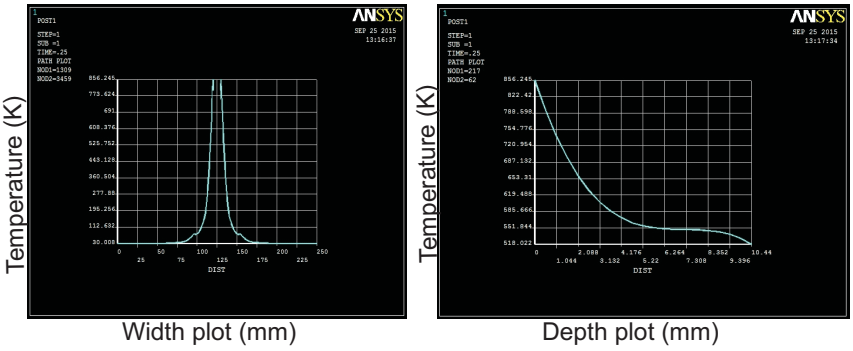

Figure 14 a)Temperature Vs Width plot of AA7075 for bead on plate weld at 140 mm/min for 0.25 sec, b) Temperature Vs Depth plot of AA7075 for weld bead geometry thickness at 140 mm/min for 0.25 sec

Fig. 13 shows the temperature distribution of bead on plate weld along with the width and depth of the plate welded at 140 mm/min. and heat input of 1.165 kJ/mm applied for 0.25 sec time step at single node and the results are captured. Fig. 14 shows the temperature versus width and depth of the welded plate graph. In this 908 K is the melting temperature of AA7075 Aluminium alloy. From Fig. 14a the bead width of 6.83 mm and Fig. 14b bead depth of 3.94 mm are identified.

6.1. *FEM analysis versus experimental results*

The weld bead geometry of AA7075 alloy is simulated using ANSYS and the arrived results are compared with the experimental results as given in Tab. 6.

The transverse temperature plots are used for finding the depth of penetration and the longitudinal plots are used to find the bead width of the weld bead. From

Table 6 Comparison of Experimental results versus Simulated results of weld bead geometry for AA7075 welded joints

Specimen No.	Weld speed mm/min	Heat input (kJ/mm)	Bead width (mm)			Bead depth (mm)		
			Exp	FEM	%Error	Exp	FEM	%Error
Sample 1	120	1.360	7.85	7.36	6.24	4.46	4.18	6.28
Sample 2	130	1.255	7.31	7.02	3.97	4.21	4.03	4.28
Sample 3	140	1.165	7.02	6.83	2.71	4.10	3.94	3.90

Tab. 6, while comparing the experimental and simulated results, the percentage of error is very less for all the 3 trials. The maximum percentage of error is found to be 6.28. Therefore, it is evident that the simulated bead width and bead depth values remain almost equal compared with the experimental values.

7. Conclusion

Based on the objective of this work, a Finite Element Method based on the transient thermal elastic plastic model has been successfully developed and applied for the welding of Aluminium Alloy 7075 sheets. The material parameters for the Aluminium Alloy 7075 material are assumed to be temperature dependent. The other phenomena like distributed arc heat input, heat loss, and so forth have been accounted in the model. The finite element analysis of the partially welded sheet has been validated through experimental trials.

The developed FEM model was simulated based on the designed matrix and various temperature contours and time temperature history plots for weld bead profile were obtained to study the effect of various weld speed on weld bead dimensions and the following conclusions were drawn:

1. Experimentally the weld trials were conducted by varying the weld speed as 120 mm/min, 130 mm/min, 140 mm/min, and the corresponding weld bead geometry was measured.

2. The experimental result shows that maximum bead width and bead depth was obtained for the samples welded at 120 mm/min.

3. For the sample welded at 130 mm/min and 140 mm/min lower heat input was applied which was insufficient. Consequently only surface melting took place which resulted in distortion in the weld plate.

4. From the experimental results it is clearly understood that heat input plays a major role in welding in which lower heat input affects the quality of the welded joints. Therefore, optimum heat input is preferred in joining of metals.

5. Comparing the experimental and simulated results reveals that the percentage of error is very less for all the 3 trials.

6. The maximum percentage of error is found to be 6.28. Therefore, it is evident that the simulated bead width and bead depth values remain almost equal compared with the experimental values.

7. If the time step is varied, the temperature distribution also varies.

8. The weld bead geometry mainly depends on the optimum weld process parameter (optimum heat input). If the applied heat input either increases or decreases from the optimum weld process parameters (optimum heat input) for the weld bead geometry decreases.

References

[1] **David, S. A. and DebRoy, T.**: Current issues and problems in welding science, *Science*, 257, 5069, 497–502, **1992**.

[2] **Zacharia, T., Vitek, J. M., Goldak, J. A., DebRoy, T., Rappaz, M. and Bhadeshia, H. K.**: Modeling of fundamental phenomena in welds, *Modelling and Simulation in Materials Science and Engineering*, 3, 2, 265–288, **1995**.

[3] **Papazoglou, V. J. and Masubuchi, K.**: Numerical analysis of thermal stresses during welding including phase transformation effects, *Journal of Pressure Vessel Technology*, 104, 3, 198–203, **1982**.

[4] **Reddy, J. N.**: On penalty function methods in the finite element analysis of flow problems, *International Journal for Numerical Methods*, 2, 2, 151–171, **1982**.

[5] **Oden, J. T., Kikuchi, N. and Song, Y. J.**: Penalty-finite element methods for the analysis of stokesian flows, *Computer Methods in Applied Mechanics and Engineering*, 31, 3, 297–329, **1982**.

[6] **McLay, R. and Carey, G. F.**: Coupled heat transfer and viscous flow, and magnetic effects in weld pool analysis, *International Journal for Numerical Methods in Fluids*, 9, 6, 713–730, **1989**.

[7] **De, A. and DebRoy, T.**: Probing unknown welding parameters from convective heat transfer calculation and multivariable optimization, *Journal of Physics, D*, 37, 1, 140–150, **2004**.

[8] **Giedt, W. H., Wei, X.-C. and Wei, S.-R.**: Effect of surface convection on stationary GTA weld zone temperatures, *Welding Journal*, 63, 12, 376–383, **1984**.

[9] **Lukens, W. E. and Morris, R. A.**: Infrared temperature sensing of cooling rates for arc welding control, *Welding Journal*, 61, 1, 27–33, **1982**).

[10] **Kovacevic, R., Zhang, Y. M. and Ruan, S.**: Sensing and control of weld pool geometry for automated GTA welding, *Journal of Engineering for Industry*, 117, 2, 210–222, **1995**.

[11] **Pitscheneder, W., Ebner, R., Hong, T., DebRoy, T., Mundra, K. and Benes, R.**: Development of a finite element based heat transfer model for conduction mode laser spot welding process using an adaptive volumetric heat source, *of the 4th International Seminar on Numerical Analysis of Weldability*,379–395, **1997**.

[12] **Rosenthal, D.**: Mathematical theory of heat distribution during welding and cutting, *Welding Journal*, 20, 5, 220–234, **1941**.

[13] **Goldak, J., Chakravarti, A. and Bibby, M.**: A new finite element model for welding heat sources, *Metallurgical Transactions B*, 15, 2, 299–305, **1984**.

[14] **Guo, W. and Kar, A.**: Determination of weld pool shape and temperature distribution by solving three–dimensional phase change heat conduction problem, *Science and Technology of Welding and Joining*, 5, 5, 317–323, **2000**.

[15] **Chang, W. S. and Na, S. J.**: A study on the prediction of the laser weld shape with varying heat source equations and the thermal distortion of a small structure in micro–joining, *Journal of Materials Processing Technology*, 120, 1–3, 208–214, **2002**.

[16] **Dutta, P., Joshi, Y. and Franche, C.**: Determination of gas tungsten arc welding efficiencies, *Experimental Thermal and Fluid Science*, 9, 1, 80–89, **1994**.

[17] **Zhang, W. , Roy, G. G., Elmer, J. W. and DebRoy, T.**: Modeling of heat transfer and fluid flow during gas tungsten arc spot welding of low carbon steel, *Journal of Applied Physics*, 93, 5, 3022–3033, **2003**.

[18] **Zhang, W., Roy, G. G., Elmer, J. W. and DebRoy, T.**: Modeling of heat transfer and fluid flow during GTA spot welding of 1005 steel, *Journal of Applied Physics*, 93, 3022–3033, **2003**.

[19] **Sathiya, P., Jinu, G. R. and Navjot Singh**: Simulation of weld bead geometry in GTA welded Duplex Stainless Steel(DSS), *Scholarly Research Exchange*, ID 324572, doi 10.3814/2009/324572, **2009**.

[20] **Durgutlu, A.**: Experimental Investigation of the Effect of Hydrogen in Argon as a Shielding Gas on TIG Welding of Austenitic Stainless Steel, *Mater. Design*, 25, 1, 19, **2004**.

[21] **Yan, J., Gao, M. and Zeng, X.**: Study on Microstructure and Mechanical Properties of 304 Stainless Steel Joints by TIG, Laser and Laser–TIG Hybrid Welding, *Opt. Laser Eng*, 48, 4, 512, **2010**.

[22] **Sathiya, P., Aravindan, S., Soundarajan, R. and Noorulhaq, A.**: Effect of Shielding Gases on Mechanical and Metallurgical Properties of Duplex Stainless–steel Welds, *J. Mater. Sci.*, 44, 1, 114, **2008**.

[23] **George, E. and Scott, D**: Hand Book of Aluminium, Volume 1&2, USA, *Marcel Dekkar Inc.*, **2003**.